Queries for apls-63-01-10

This manuscript/text has been typeset from the submitted material. Please check this proof carefully to make sure there have been no font conversion errors or inadvertent formatting errors. Allen Press.

Noninvasive Mail Inspection System with Terahertz Radiation

HIROMICHI HOSHINA,* YOSHIAKI SASAKI, AYA HAYASHI, CHIKO OTANI, and KODO KAWASE

Riken, 519-1399 Aramaki-Aoba, Aoba-ku, Sendai, Miyagi, 980-0845, Japan; and Nagoya University, Furo-cho, Chikusa-ku, Nagoya, 464-8603, Japan

Using the high penetrability of the terahertz waves and the characteristic absorption spectra in this frequency range, we have built a noninvasive mail inspection system targeting drugs and explosives. The system is composed of two stages; in the first stage, the scattering of a continuous terahertz wave is used for selecting mail that contains concealed powder; in the second stage, the absorption spectrum of the suspicious mail is measured and the material is identified using a terahertz spectrum database. We evaluated the performance and the limits of the inspection system.

Index Headings: **Terahertz wave; Drug analysis; Explosives analysis; Fingerprint spectrum; Mail; Spectroscopy.**

INTRODUCTION

Due to the recent developments in the generation and detection techniques for terahertz (THz) electromagnetic waves, various applications using THz waves have been proposed.[1] The THz radiation lies approximately in the frequency range from 0.1 to 10 THz (wavelength from 3 mm to 30 μm) and shows properties of both radio waves and optical light. Because of its longer wavelength, THz waves are less scattered by soft materials such as paper, wood, and plastics and can create images of the objects packed in those materials. On the other hand, many materials show particular absorption spectra in the THz region that can be used for their identification. Therefore, THz waves are a good inspection and identification tool for materials concealed in envelopes, plastic bags, and cardboard boxes.

Security and safety-related applications are currently strongly required because of the recent social and political situation in the world. One such application is the inspection and detection of illicit drugs and hazardous materials inside mail. In Japan, the inspection of private mails is restricted by law and noninvasive inspection such as X-ray imaging and dogs are used for detecting hidden drugs. However, X-ray cannot identify the materials and dogs can smell drugs only when the vapor of a drug is leaking from the package. In 2003 Kawase et al. found that the THz wave can be used for the identification of materials in envelopes without opening the package.[2] Since then, many applications for security and safety have been developed utilizing THz waves.[3–7]

In this paper, we describe a prototype apparatus that can identify these substances concealed inside mail without opening it by taking advantage of the properties of THz waves. For the inspection, we have proposed the following procedure. First, the measurement of scattered THz waves is applied to pick up suspicious mail because the scattering is a good indicator of the presence of powder inside an envelope. Second, the identification of the chemical substances in the suspicious mail is achieved with a THz time-domain spectrometer using a THz fingerprint spectrum database. We built a prototype apparatus for post offices and evaluated the performance and the limits of the inspection system.

TERAHERTZ RAPID SCREENING SYSTEM

Our project aims at inspecting all mail handled in the Japanese international post offices, that is, more than 100 000 postal items a day. However, taking into account the speed limits of the THz spectrometer, it is impossible to measure the spectra of all of them. To achieve, however, a complete inspection, the process was segmented into two stages; the first stage makes a rapid screening and the second stage identifies the substances in the mail selected as suspicious in the first stage. For rapid screening, we detect the scattering of the THz waves from powders as the THz waves are intensely scattered when the particle size is comparable to the wavelength.[8]

Figure 1a shows the schematic figure of the rapid screening stage. Envelopes are conveyed by a belt with a speed of 100 meters per minute and scanned by an X-ray line camera and the THz scattering detector. The thickness of the envelopes is mechanically limited to 20 mm. In this apparatus, X-ray images of all envelopes are taken (II). Envelopes containing only paper, which appears flat and transparent in the X-ray images, are removed from the conveyor belt (III), while those with shadow areas are sent to the next step. For the THz scattering detector, which can measure only a single position at a time, the horizontal position of the envelopes is adjusted (IV) so that the area recorded as a shadow in the X-ray is brought into the focal point of the THz scattering detector (V).

Figure 1b shows the optical setup of the THz scattering detector. A Schottky barrier diode (Virginia Diode Inc.) was used as a continuous wave source with a frequency of 540 GHz and power of 0.7 mW. The THz continuous beam was collimated by a plastic lens and focused on the surface of the envelopes with an incident angle of 45°. Two plastic lenses are placed in the vertical direction under the focal point to collect the THz waves scattered from the envelopes, and then focus them on the Schottky barrier diode detector (WR-1.5ZBD Virginia Diode Inc.). Note that the optics are aligned so as to prevent the direct reflection from the surface of the envelopes from arriving at the detector. The amplitude of the THz wave was modulated at 30 kHz through the bias voltage and the signal was detected with a lock-in amplifier. The conveyor stops at the position in which the THz focus falls on the shadow area of the X-ray image, and the THz scattering is measured. During the measurement, the conveyor stops for 0.3 s and the signal is integrated for a better signal-to-noise ratio. When more than one area is found in the X-ray image, the conveyer carries the envelope back to the stage (IV) to reposition it in the horizontal direction and then again to stage (V) to measure the next area.

Received 10 July 2008; accepted 22 October 2008.
* Author to whom correspondence should be sent. E-mail: hoshina@ricken.jp.

0003-7028/09/6301-000000$2.00/0

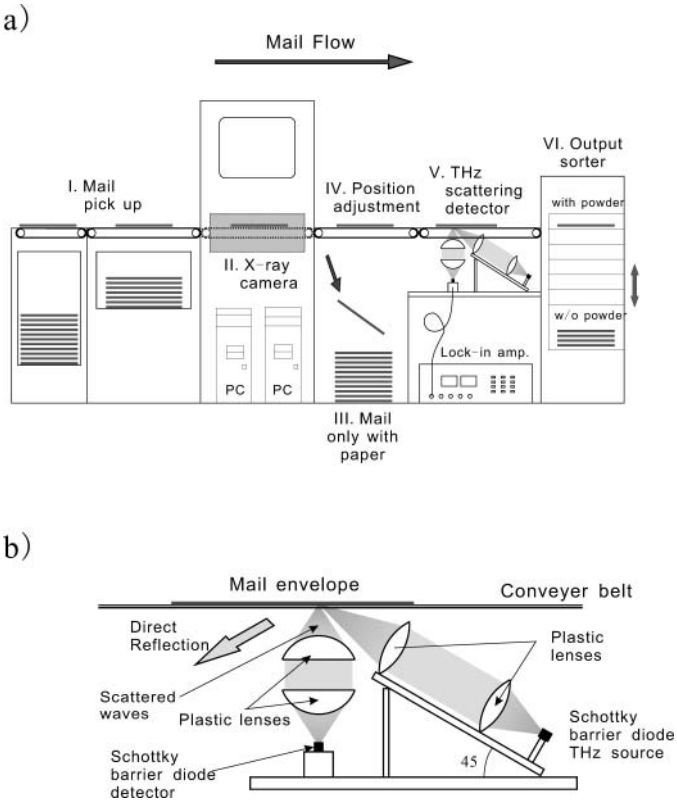

FIG. 1. Schematic of (**a**) the THz rapid screening system and (**b**) the optical setup of the THz scattering detector.

Figure 2 shows the power of the scattered THz wave at various particle sizes in the case of sucrose powder. For this measurement, the source was a Schottky barrier diode at 600 GHz and 70 μW (Virginia Diode Inc.) and the detector was a DLATGS pyroelectric sensor (JASCO Co.), in the same optical setup. The sucrose powders were prepared by sieving through different mesh sizes, from 90 μm to 1 mm. The average particle size and its standard deviation were obtained by visual measurement with a microscope. Sucrose powder packed in polyethylene bags was inserted in envelopes and placed at the focal point of the scattering detector. The scattering from the envelope was also measured and is plotted at the right side of Fig. 2.

At particle sizes below 500 μm, the scattering power monotonically increases with the particle size. From Mie's scattering theory, the extinction also increases at $\pi a(n-1) < \lambda$, where λ is the wavelength, a is the particle radius, and n is the refractive index of the particle.[8] The solid and dashed lines in Fig. 2 show the extinction curve obtained from Mie's theory with non-absorbing spheres and partially absorbing spheres,[8] respectively, by assuming the refractive index of powder to be 1.3. The amplitude of the curves is scaled arbitrarily. The behavior of the scattered power is in better agreement with the model with partially absorbing spheres. The result shows that even the finest powder (90 μm) gives significantly more scattering signal than the envelope without powder, so the powder inside the envelope is detectable from the THz scattering signal. Using these results, the rapid screening system selects the envelopes showing strong THz scattering as suspicious mail. The position of the powder packet is recorded

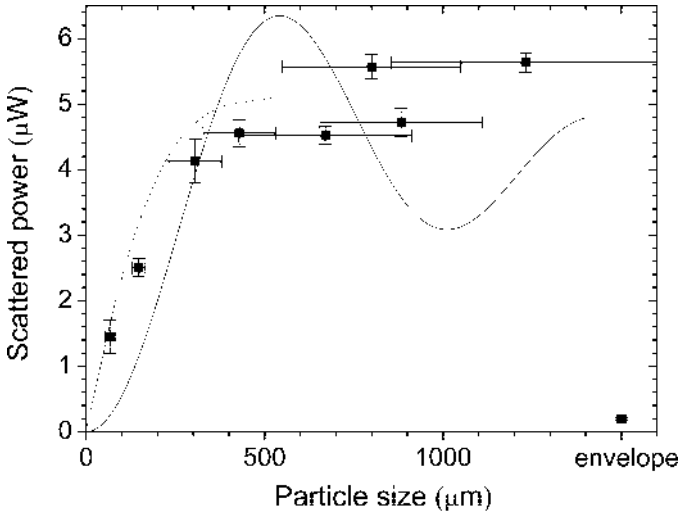

FIG. 2. THz scattering signal intensity of sucrose powder with different particle sizes and envelopes measured with a 600 GHz source. The error bars show the standard deviation of the particle size and of the detected signal. The solid and dashed lines show the extinction curves obtained by the Mie scattering model.

and the suspicious mail is stored in the sorter (IV) and transferred to the next stage.

TERAHERTZ TIME-DOMAIN SPECTROMETER

The THz absorption spectra of the suspicious mail selected by the rapid screening system were measured with a terahertz time-domain spectrometer (THz-TDS). THz-TDS is a recently developed spectroscopic technique available for the THz region that uses a femtosecond pulse laser for the generation and the detection of THz waves.[1,9,10] Since the THz-TDS directly measures the electric field of the THz waves with short laser pulses, the system is less affected by thermal noise at 300 K and achieves high sensitivity without liquid He cooling.[11] Therefore, the THz-TDS is the most appropriate spectrometer for use in this wavelength region, as well as for use outside the laboratory.

For the purpose of this project, we modified the standard THz-TDS as follows.

To avoid movement of the powder package inside the envelopes, the mail was placed horizontally during the measurement. Therefore, the THz optics were oriented vertically.

The THz waves are strongly absorbed by the water vapor in the atmosphere. To avoid this problem, the THz optics were placed in a chamber purged by nitrogen gas, as shown in Fig. 3, while the envelope is placed between two plastic windows to exclude the surrounding air from the optical path.

In order to use the femtosecond laser stably, the temperature and the humidity inside the system was controlled by an air conditioning system.

Due to the daily changes in the system environment, the optical path of the laser might become misaligned. To compensate for this, a computer-controlled adjustable mirror was introduced in the laser optics to maintain an intense THz signal. The alignment is optimized automatically on a daily basis.

Figure 3 shows a schematic and a photograph of the spectrometer. A mode-locked Ti:Sapphire laser (INTEGRAL

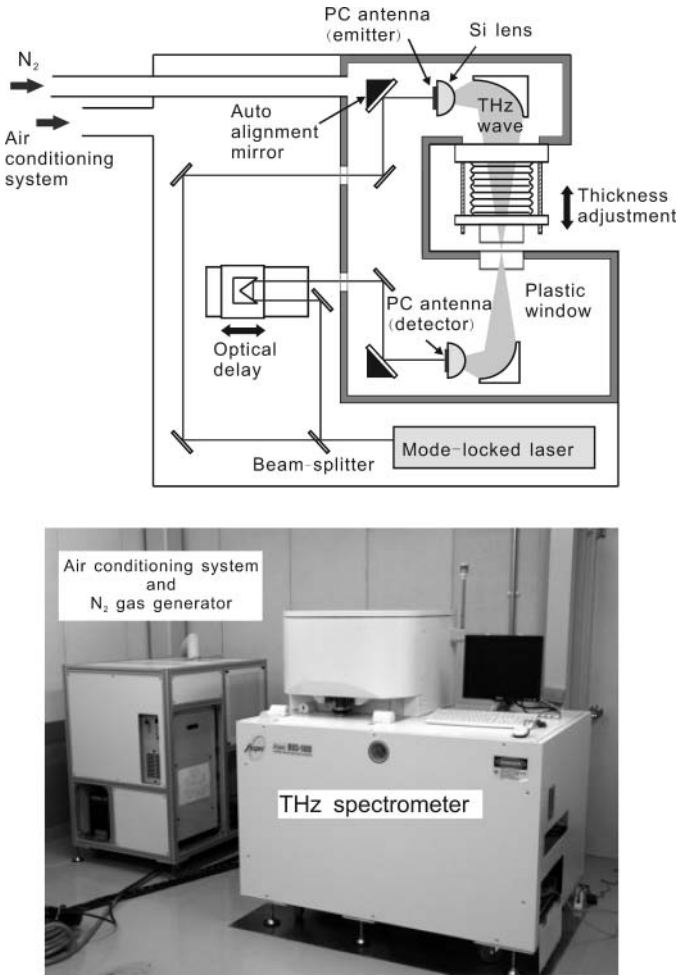

FIG. 3. Schematic and photograph of the THz-TDS system.

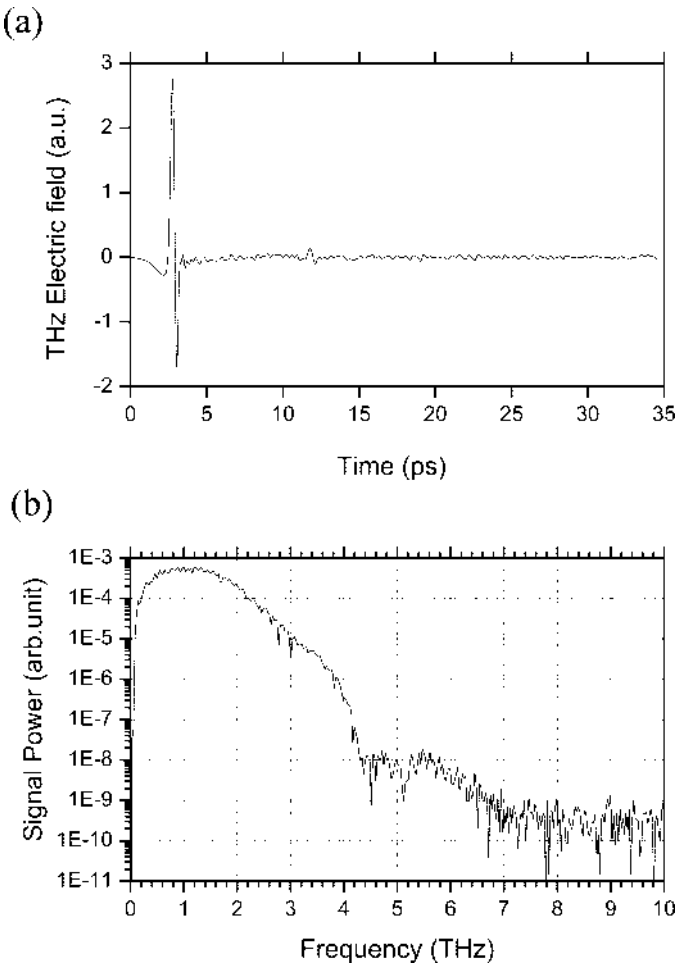

FIG. 4. An example of (**a**) the THz time-domain waveform and (**b**) its power spectrum measured without sample.

PRO Femtolasers Co.) with a pulse width of 10 fs, a repetition rate of 85 MHz, and an output power of 100 mW was used for generation and detection of pulsed THz waves. The laser beam was divided by a beam-splitter into a pump and a probe beam. The pump beam was focused onto the gap of a dipole-type GaAs photo-conductive (PC) antenna with a bias voltage of 50 V. The production and extinction of photo carriers at the antenna causes a single-cycle electric field with a time length of 1 ps, which corresponds to a broadband radiation, from 0.1 to 6 THz. The THz radiation emerges from the silicon super-hemispherical lens attached to the antenna substrate and is focused by an elliptical mirror to the center of the THz window; it is then focused again on the other PC antenna, used as a detector. The amplitude of the transmitted THz electric field at the moment when the probe laser pulse reaches the detector is determined from the measurement of the output current caused by the movement of the photo carriers produced by the probe pulse. The bias voltage of the emitter antenna is modulated and the output current from the detector antenna is pre-amplified and then lock-in amplified in order to reduce the low frequency system noise.

The THz time-domain waveform is recorded by scanning the time delay of the probe pulse with an optical delay stage. The time-domain data was recorded for 35 ps, which corresponds to a frequency resolution of 0.96 cm^{-1}. Multiple scans (20 times) are applied in an interval of two minutes and the time-domain waveforms are averaged over the scans. Then the time-domain waveform is Fourier transformed and the THz power spectrum is obtained. Figures 4a and 4b show, respectively, an example of a THz time-domain waveform and its power spectrum measured without a sample. The pulsed THz radiation is observed at 3 ps as a single cycle electric field. Note that the small peak around 12 ps is the Fresnel reflection inside the PC antenna, which can be removed when the sample spectrum is converted to absorbance. The THz power shows a maximum around 1.4 THz and then gradually decreases at higher frequencies, reaching a noise level around 7 THz. Taking the detection noise level as $10^{-9.5}$, the dynamic range of the spectrometer is estimated to be 10^6 between 0.5 and 2 THz, and $10^{4.5}$ at 3 THz.

The absorbance of the sample $\alpha(\omega)$ is calculated as

$$\alpha(\omega) = -\log_{10}[I_{sa}(\omega)/I_{ref}(\omega)] \quad (1)$$

where $I_{sa}(\omega)$ is the sample spectrum and $I_{ref}(\omega)$ is the reference spectrum. This non-dimensional representation was used in all measurements shown in this work.

Since the system is stable and the parameters of the spectrometer do not change quickly, the same reference spectrum measured at the beginning of the day can be used for every measurement in that day. From the dynamic range of

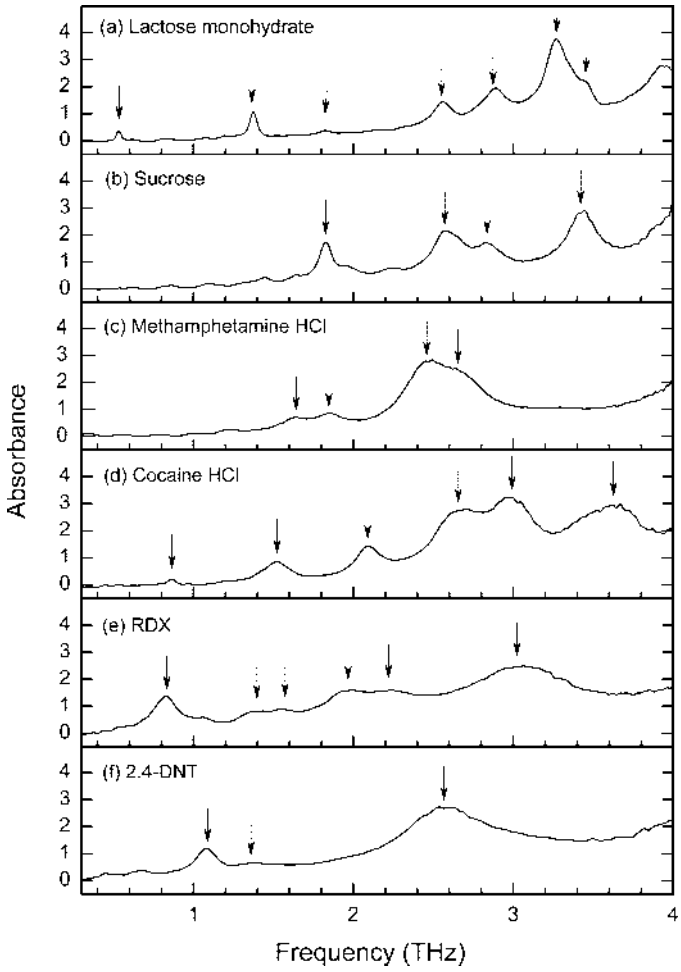

FIG. 5. THz absorption spectra of (**a**) lactose monohydrate, (**b**) sucrose, (**c**) methamphetamine HCl, (**d**) cocaine HCl, (**e**) RDX, and (**f**) 2,4-DNT packed with polyethylene films. The samples are measured after being sieved and the average particle size is below 100 μm.

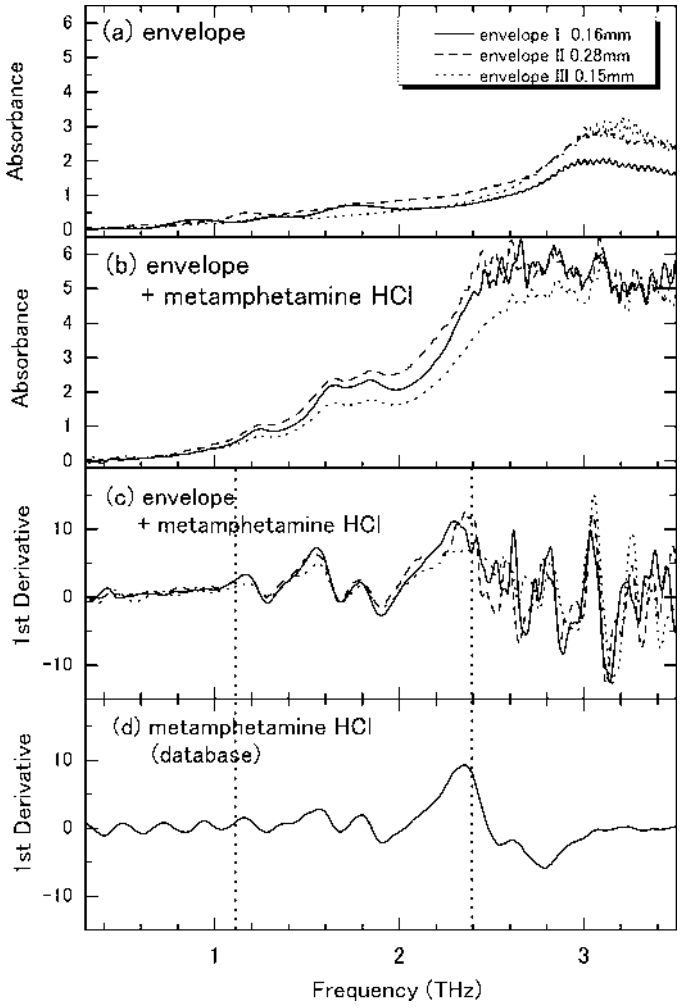

FIG. 6. (**a**) THz absorption spectra of envelopes with a thickness of (I) 0.15 mm, (II) 0.28 mm, and (III) 0.16 mm. (**b**) THz absorption spectrum of methamphetamine HCl with a particle size of 170 μm packed with polyethylene films and inserted in an envelope, and (**c**) its first derivative. (**d**) The first derivative of the database spectrum of methamphetamine HCl.

the spectrometer, the measurable absorbance is estimated as up to 6 in the range 0.5–2 THz and up to 4.5 at 3 THz.

MATERIAL IDENTIFICATION

For the identification of chemicals, we built a spectral database in the THz region. The spectra of more than 40 chemicals have been measured. Most of them show clear fingerprint spectra in the THz region. The samples were packed in bags made of polyethylene films with a thickness of 0.11 mm and the THz absorption spectra were measured. About 100 mg of the sample was sealed in the packet and the total thickness of the sample was about 0.5 mm. Before packing the samples, chemicals were ground and sieved to a particle size below 100 μm in order to minimize the scattering. Figure 5 shows some examples of THz absorption spectra measured for the database. Spectra of widely used chemicals (lactose monohydrate 100% and sucrose 100%, Wako Pure Chemical Industries, Ltd.), drugs (methamphetamine HCl 100%, Dainippon Sumitomo Pharma Co., Ltd., and cocaine HCl 100%, Takeda Pharmaceutical Co., Ltd.), and explosives (trimethylenetrinitramine (RDX) and 2,4-dinitrotoluene (DNT)) are shown. The arrows at in the spectra show the characteristic absorption features of the chemicals, which are consistent with previous works.[2,4,6,7] Since the number of peaks, positions, and line shapes is different in different chemicals, the spectra can be used for the identification of the material. The agreement between the measured spectra and the database is evaluated using the correlation coefficient between the first derivatives of those spectra. The first derivative is taken to remove the baseline slope and clarify the spectral features. The Savitzky–Golay algorithm with filtering of 15 points is used for the calculation. The number of filtering points is determined so as not to lose the characteristic spectral features (typically with the line width of 0.2 THz). The correlation coefficient R was calculated as follows,

$$R = \frac{\sum (X_i - X_{\text{ave}}) \cdot (Y_i - Y_{\text{ave}})}{\sqrt{\sum [(X_i - X_{\text{ave}})]^2} \sqrt{\sum [(Y_i - Y_{\text{ave}})]^2}} \qquad (2)$$

where X_i and Y_i are the ith data of the measured spectra and database, and X_{ave} and Y_{ave} are their average.

Figure 6 shows absorption spectra of several envelopes, an example spectrum of methamphetamine HCl with particle size

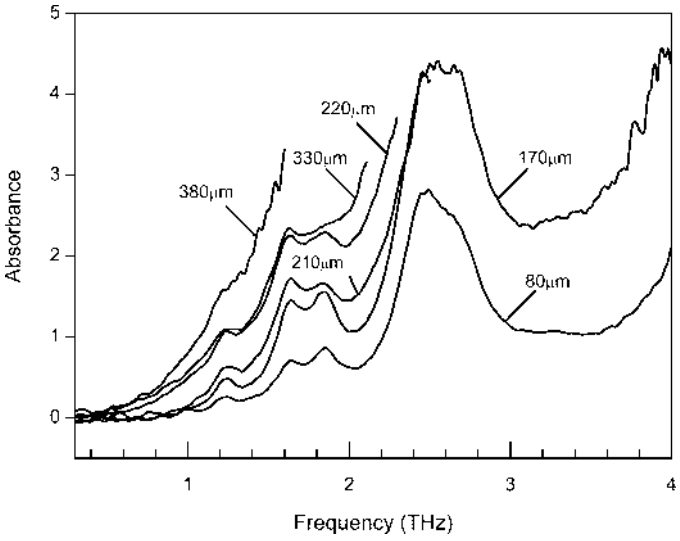

FIG. 7. THz absorption spectra of methamphetamine HCl powder with various particle sizes.

of 170 μm concealed in envelopes, their first derivative, and the first derivative of the database spectrum of methamphetamine HCl. The thickness of the samples is about 0.5 mm. Three kinds of envelopes are used in this example: envelopes I and II are paper envelopes in general use in Japan with thicknesses of 0.16 and 0.28 mm, respectively, and envelope III is a plastic envelope with a thickness of 0.15 mm. All envelopes show small absorption features below 2 THz and a strong absorption around 3 THz. From the thickness of the envelopes, the waving below 2 THz can be understood as optical fringes due to the multiple reflection inside the paper. On the other hand, a broad strong absorption around 3 THz is seen in all samples.

Due to the difference in the envelope absorbance and scattering, and small differences in the sample thickness, the three spectra in Fig. 6b show different absorbance. However, after taking the first derivative, the differences vanish and the spectral features of the methamphetamine HCl remain. It is seen that the spectral features of Fig. 6c show a good agreement with Fig. 6d in the frequency range from 1.1 to 2.4 THz. The appropriate frequency range for calculating the correlation coefficients depends on the sample and package, and we determined the range based on the absorption intensity of the spectrum (discussed in the next section). In this case, the data points from 1.1 to 2.4 THz are used, and the correlation coefficients of these spectra are 0.91, 0.89, and.0.84, respectively.

In this project, all the procedures for spectral analysis and database retrieval described above are automatically executed by the software. After the measurement, a list of the possible chemical names of materials is displayed immediately on the screen based on the value of the correlation coefficient. The measurement and identification is automatically executed by the computer and special knowledge is not necessary for the system operation.

DISCUSSION

For the use of the system in real-life situations, the system should work for a variety of packages and materials. Two important factors determine the accuracy of the material identification: optical interference and scattering.

Optical interference occurs by Fresnel reflection at the interfaces between materials. Generally, it is stronger when the difference of the refractive indices of materials is larger and when the extinction in the material is smaller. As visible in Fig. 6a, the spectrum of envelope I has fringes with a period of about 0.8 THz. Assuming the refractive index of paper is 1.3, the back and forward propagation in a paper with thickness of 0.16 mm corresponds to an optical length of 0.42 mm. As a result, the period of the fringe becomes 0.7 THz, which is in good agreement with the observed data. The optical interference seriously affects the correlation coefficient when the period of the fringe is close to the line width of the characteristic peaks. For example, an air gap with a thickness of 0.8 mm will have severe effects on the spectra.

To minimize this effect, the thickness adjustment mechanics of the spectrometer presses the envelope to diminish the air gaps. Also, the refractive index of the plastic window is close to that of paper and minimizes the Fresnel reflection at the interface between the window and the envelope. However, in some cases, strong fringes appear on the spectra. The periodical oscillation appearing in the frequency region from 0.3 to 1.2 in Fig. 6d is due to the optical interference in the sample (thickness is about 0.5 mm). Since the period of the fringe is 0.2 THz, it could not be removed by the first derivative. In this case, the fringes appear stronger at the lower frequency region because the extinction of the THz waves in the sample is stronger as the frequency becomes higher because of the absorption and scattering of the sample. In fact, the fingerprint spectra beyond 1.2 THz can be clearly recognized in Fig. 6d.

Thus, the optical interference changes the spectra and makes the material identification difficult. However, the fringe shape and strength highly depend on the sample structure and are difficult to predict for actual mail. In order to minimize the inference of optical fringes in the correlation coefficients, we removed data below 1.1 THz in which the amplitude of the fringe is stronger and most chemicals show no fingerprint spectra.

The optical scattering by the sample determines the higher frequency limit. Figure 7 shows the effect of particle size on the absorption spectrum of methamphetamine HCl. As the particle size becomes larger, the scattering at the higher frequency become stronger and the measurable frequency limit becomes lower. When the particle size is less than 200 μm, we can recognize the fingerprint spectra up to 3 THz, but this is difficult when the particle size is larger.

Since the packages increase the absorption of the actual contents, their measurable frequency limit may become lower. To exclude the saturated data from the calculation of the correlation coefficient, we removed the data in which the sample spectrum $I_{sa}(\omega)$ becomes lower than the noise level. On the other hand, the range has to be wide enough for the material identification, that is, it must include characteristic peaks of the fingerprint spectra. For example, when we target methamphetamine HCl, its characteristic peaks appear at 1.2, 1.6, 1.8, and 2.4 THz. At least three peaks have to be included in the frequency region in order to distinguish the correlation coefficient of methamphetamine HCl from those of the other materials. In this case, we set the required frequency range as 1.1–2.1 THz.

As discussed above, the sample thickness and particle size are limited. In the case of methamphetamine HCl, the limit of the thickness is about 2 mm when the particle size is 170 μm

and the sample is wrapped in paper (envelope I). On the other hand, the upper limit of the particle size is about 220 μm when the sample thickness is about 0.5 mm. According to the lower limit of the detectable particle size of the rapid screening system, the suitable range of the particle size for the total system is from 90 to 220 μm.

CONCLUSION

In this paper, we have presented a prototype apparatus that can identify illicit substances concealed inside the mail without opening it. A combination of an X-ray camera and a THz scattering detector enables the rapid screening of mail and selects those envelopes containing powder. The THz-TDS measures the spectra of the envelope and its contents and identifies the chemicals concealed inside by using THz fingerprint spectra. The comparison of the spectrum with the THz database is automatically executed using the correlation coefficient, without requiring the operator to have special knowledge.

ACKNOWLEDGMENTS

The authors wish to thank Aispec Co. Ltd. and Manta Ware Inc. for their efforts and discussion towards refining the THz spectroscopic system. The authors also thank SI Seiko Co. Ltd. for their efforts in building the THz rapid screening system. Also, the authors would like to thank Dr. Adrian Dobroiu for his kind advice for this article. This work was partially supported by the Special Coordination Funds for Promoting Science and Technology in the Japanese Ministry of Education, Culture, Sports, Science and Technology (MEXT).

1. D. L. Woolard, W. R. Loerop, and M. S. Shur, *Terahertz Sensing Technology: Emerging Scientific Applications & Novel Device Concepts* (World Scientific Publishing, Singapore, 2004).
2. K. Kawase, Y. Ogawa, and Y. Watanabe, Opt. Exp. **11,** 2549 (2003).
3. W. H. Fan, A. Burnett, P. C. Upadhya, J. Cunningham, E. H. Linfield, and A. G. Davies, Appl. Spectrosc. **61,** 638 (2007).
4. K. Yamamoto, M. Yamaguchi, F. Miyamaru, M. Tani, M. Hangyo, T. Ikeda, A. Matsushita, K. Koide, M. Tatsuno, and Y. Minami, Jpn. J. Appl. Phys. **43,** L414 (2004).
5. T. Ikeda, A. Matsushita, M. Tatsuno, Y. Minami, M. Yamaguchi, K. Yamamoto, M. Tani, and M. Hangyo, Appl. Phys. Lett. **87,** 034105 (2005).
6. J. F. Fedrici, B. Schulkin, F. Huang, D. Gary, R. Barat, F. Oliveira, and D. Zimdars, Semicond. Sci. Technol. **20,** S266 (2005).
7. H. Zhong, A. Redo-Sanchez, and X.-C. Zhang, Opt. Exp. **14,** 9130 (2006).
8. H. C. v. d. Hulst, *Light Scattering by Small Particles* (Dover Publications, New York, 1981).
9. M. v. Exter and D. R. Grischkowsky, IEEE Trans. Microwave Theory Technol. **38,** 1684 (1990).
10. M. Exter, C. Fattinger, and D. Grischkowsky, Opt. Lett. **14,** 1128 (1989).
11. P. Y. Han, M. Tani, M. Usami, S. Kono, R. Kersting, and X. C. Zhang, J. Appl. Phys. **89,** 2357 (2001).